Published in IET Generation, Transmission & Distribution
Received on 10th March 2012
Revised on 23rd October 2012
Accepted on 31st October 2012
doi: 10.1049/iet-gtd.2012.0357

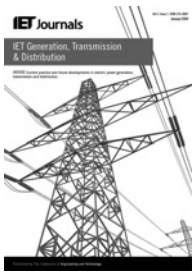

ISSN 1751-8687

Subsynchronous resonance mitigation using variable-speed wind energy conversion systems

Andres Enrique Leon[1], Juan Manuel Mauricio[2], Jorge Alberto Solsona[1]

[1]*Instituto de Investigaciones en Ingeniería Eléctrica (IIIE) 'Alfredo Desages' (UNS-CONICET), Universidad Nacional del Sur (DIEC-UNS), Avenida Alem 1253, Bahía Blanca 8000, Argentina*
[2]*Department of Electrical Engineering, University of Seville, 41092 Seville, Spain*
E-mail: aleon@ymail.com

Abstract: This work proposes a strategy to mitigate subsynchronous resonance (SSR) in synchronous generators using variable-speed wind energy conversion systems (WECSs) based on full converter wind turbines. A supplementary active and reactive power to be delivered by WECSs located near synchronous generators is designed to reduce the SSR phenomenon. These supplementary signals are calculated using an observer-based controller tuned through an optimal quadratic technique which allows to minimise the WECS control effort, whereas a good torsional oscillation damping is accomplished. The power ratio between the WECS and the synchronous generator, impact on the power quality and communication time-delay requirements are also discussed. The authors compare two control approaches: the first one uses mechanical measurements of the synchronous generator (measures which have high observability of torsional modes), whereas the second one uses voltage measurements at the wind farm connection point. In this way, two control schemes using remote and local measurements are proposed, and advantages and disadvantages of both schemes are presented. The proposed scheme can provide satisfactory torsional damping under a wide range of operating points, avoiding to include dedicated SSR damping equipment, and using the new wind farms installed in the network. Eigenvalue analysis and non-linear time-domain simulations confirm the good performance of the WECS-based SSR damping controller.

1 Introduction

Wind energy conversion systems (WECSs) based on power ac/dc converters are now a mature technology in power systems [1]. Because of their growing penetration and power control flexibility, they are subject to several network support tasks [2] involving: voltage control [3], transient frequency regulation [4, 5] and stability enhancement [6]. In this work, we study a new WECS supplementary action to mitigate subsynchronous resonance (SSR) when WECSs are located near synchronous generators. SSR is a phenomenon which may occur in thermal power plants closely connected to series-compensated transmission lines. If a mechanical torsional mode of the turbine multi-mass system coincides with, or is close to, an electrical network mode (described in the rotating coordinates), then large magnitude torques and poorly damped oscillations arise in the generator rotor. These oscillations lead to fatigue damage, life-time reduction, electrical instability, and even failures in the turbine-generator shaft. Owing to economic reasons and an increasing demand, series compensation of long transmission lines is frequently applied to enhance power transfer. However, although this technique is an important way to improve power transfer capability, it may lead to SSR phenomenon [7, 8]. Subsynchronous oscillations were first discussed in 1937 [9], but it was not until the 70s (when two shaft failures took place in the Mohave plant, in December 1970 and October 1971 [10]) that several studies and solutions were carried out to mitigate the SSR condition.

In each particular case, considering the probability of SSR and the level of expected damage, a cost effective countermeasure should be proposed. This can range from simply generator tripping to a more costly inclusion of flexible ac transmission systems (FACTS) [7]. Several SSR damping approaches based on different devices can be found in the literature, such as

- Thyristor switched resistor (NGH scheme) [11];
- Thyristor-controlled series capacitor (TCSC) [12–15];
- Gate-controlled series capacitor (GCSC) [16];
- Static synchronous series compensator (SSSC) [17–20];
- Static VAR compensator (SVC) [21–23];
- Static synchronous compensator (STATCOM) [24–26];
- Superconducting magnetic energy storage (SMES) [27];
- Voltage source converters (VSC)-based HVDC transmission system [28];
- Unified power-flow controller (UPFC) [29];
- Interline power-flow controller (IPFC) [30].

Most of these FACTS-based approaches are expensive and, unless they use big energy storage systems, series converters can only inject a quadrature voltage, and shunt converters can only inject a quadrature current (reactive power).

Considering the above drawbacks and the increase of wind farms in the grid, we propose to use variable-speed WECSs based on full converter wind turbines placed near synchronous generators to reduce the risk of SSR. WECSs have an advantage over FACTS when fast active power injection is required [1, 31, 32]. Features like speed and stored energy are naturally found in WECSs, which can resort to the kinetic energy stored in the rotational masses through power electronics and, at the same time, inject reactive power. These characteristics give the WECS-based SSR mitigation an advantage against traditional approaches.

The ability to damp SSR oscillations using WECSs is researched in this article. Two schemes to build the SSR damping controller are presented: one of them using speed measurements of the synchronous generator, and the other using a local voltage measurement at the wind farm connection point. Several implementation issues are also discussed, such as: the power ratio between the WECS and the synchronous generator, communication time-delay requirements, advantages and disadvantages of considering remote and local measurements, and the impact on the power quality of the grid.

The paper is organised as follows. Section 2 introduces the model of power system case study. The SSR damping controller is developed in Section 3. The measurement selection is discussed in Section 4. Section 5 presents the controller performance assessment, discussions and tests. Finally, conclusions are given in Section 6.

2 Power system model

The power system used in this study is the IEEE second benchmark model (case 1) for SSR analysis [33]. All models and parameters are in a per-unit system and are extracted from [33] (see Table 1). A modification to the network is made to include a variable-speed WECS, as it can be seen in the single-line diagram in Fig. 1.

2.1 Electrical model of the synchronous generator

The electrical model of the synchronous generator is described in the synchronous reference frame (SRF), and consists of two stator winding (d,q) and four rotor circuits which model the field winding (F), one d-axis damper winding (D) and two q-axis damper windings (Q,G). A field excitation system, automatic voltage regulator (AVR), and power system stabilizer (PSS) with a torsional filter, designed following the recommendations of [34, 35], have also been included. A block diagram of the implemented excitation system is shown in Fig. 2.

2.2 Mechanical model of the synchronous generator

We consider a mechanical system of the synchronous generator consisting of four lumped masses (high-pressure turbine, low-pressure turbine, generator rotor and exciter) connected through a nonrigid shaft (see block called 'synchronous generator mechanical system' in Fig. 3). The dynamics of the multi-mass mechanical system based on a mass-spring-damping model [8, 36] is given by

$$\dot{\boldsymbol{\theta}} = \Omega_{\mathrm{Br}}\boldsymbol{\omega} \tag{1}$$

$$2\boldsymbol{H}\dot{\boldsymbol{\omega}} = \boldsymbol{\tau} + \boldsymbol{K}\boldsymbol{\theta} + \boldsymbol{D}\boldsymbol{\omega} \tag{2}$$

Table 1 Power system parameters and data

Description	Symbol	Value
Synchronous generator (electrical parameters)		
base power	S_{B}	600 MVA
base voltage (line-to-line RMS)	V_{B}	22 kV
base angular frequency	Ω_{B}	2π60 r/s
stator winding resistance	R_{s}	0.0045
leakage inductance	L_{l}	0.14
d-axis inductance	L_d	1.65
q-axis inductance	L_q	1.59
field winding resistance	R_{F}	0.00096
field winding inductance	L_{F}	1.629
D-axis damper winding resistance	R_D	0.016
D-axis damper winding inductance	L_D	1.642
G-axis damper winding resistance	R_G	0.00897
G-axis damper winding inductance	L_G	1.861
Q-axis damper winding resistance	R_Q	0.0116
Q-axis damper winding inductance	L_Q	1.524
Excitation system (AVR, PSS and torsional filter)		
amplifier stage gain	K_{A}	200
amplifier stage time constant	T_{A}	0.01 s
transducer time constant	T_{R}	0.015 s
minimum excitation voltage limit	$E_{fd}^{\min}$	−6
maximum excitation voltage limit	$E_{fd}^{\max}$	6.5
PSS gain	K_{S}	20
Washout time constant	T_{wo}	10 s
PSS phase compensation time constant	T_1	0.05 s
PSS phase compensation time constant	T_2	0.02 s
PSS phase compensation time constant	T_3	3 s
PSS phase compensation time constant	T_4	5.4 s
stabilizer output limits	$V_{\mathrm{ST}}^{\max}$	±0.20
notch frequency of the torsional filter	ω_0	2π24.6 r/s
low-pass frequency of the torsional filter	ω_1	$0.65\omega_0$
damping of the torsional filter	ξ	0.2
Steam turbine multi-mass system		
exciter inertia constant	H_1	0.0069 s
generator inertia constant	H_2	0.879 s
low-pressure turbine inertia constant	H_3	1.551 s
high-pressure turbine inertia constant	H_4	0.249 s
exciter damping	D_1	0.00138
Generator damping	D_2	0.176
low-pressure turbine damping	D_3	0.3103
high-pressure turbine damping	D_4	0.0498
exciter/generator spring constant	K_{12}	3.7398
generator/low-pressure turbine spring constant	K_{23}	83.459
low-/high-pressure turbine spring constant	K_{34}	42.697
Electrical network parameters (on a 100 MVA base)		
resistance from bus 1 to bus 3	R_{13}	0.0014
inductance from bus 1 to bus 3	L_{13}	0.03
resistance from bus 2 to bus 3 (first line)	R_{23a}	0.0074
inductance from bus 2 to bus 3 (first line)	L_{23b}	0.08
resistance from bus 2 to bus 3 (second line)	R_{23b}	0.0067
inductance from bus 2 to bus 3 (second line)	L_{23b}	0.0739
generator step-up transformer resistance	$R_{2\mathrm{T}}$	0.0002
generator step-up transformer inductance	$L_{2\mathrm{T}}$	0.02

Except where indicated, parameters are in the per-unit system.

where $\Omega_{\mathrm{Br}} = (\Omega_{\mathrm{B}}/N_{\mathrm{r}})$ is the base angular speed of the generator rotor and the following vectors are defined

$$\boldsymbol{\theta} \triangleq \begin{bmatrix} \theta_1 & \theta_2 & \theta_3 & \theta_4 \end{bmatrix}^{\mathrm{T}} \tag{3}$$

$$\boldsymbol{\omega} \triangleq \begin{bmatrix} \omega_1 & \omega_2 & \omega_3 & \omega_4 \end{bmatrix}^{\mathrm{T}} \tag{4}$$

$$\boldsymbol{\tau} \triangleq \begin{bmatrix} 0 & -T_{\mathrm{e}} & \frac{T_{\mathrm{m}}}{2} & \frac{T_{\mathrm{m}}}{2} \end{bmatrix}^{\mathrm{T}} \tag{5}$$

Vectors $\boldsymbol{\theta}$ and $\boldsymbol{\omega}$ have the absolute angles and angular speeds of each lumped mass. The vector $\boldsymbol{\tau}$ stands for the external torques

doi: 10.1049/iet-gtd.2012.0357

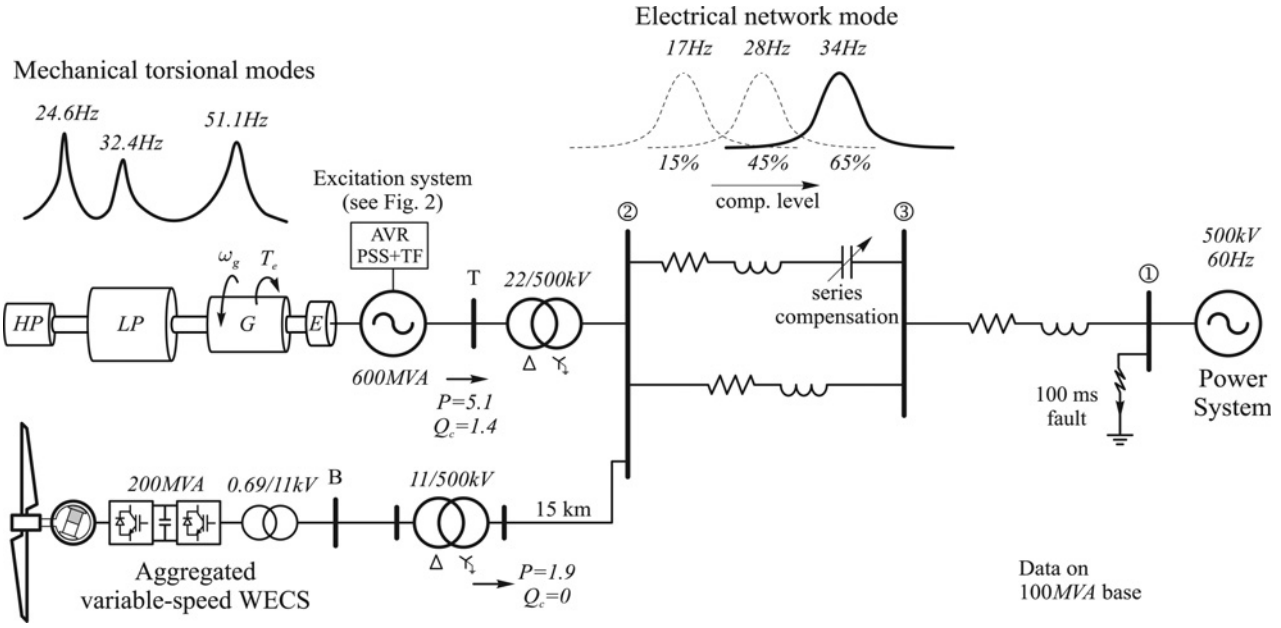

Fig. 1 *Single-line diagram of the studied system with WECS (based on the IEEE second benchmark model)*

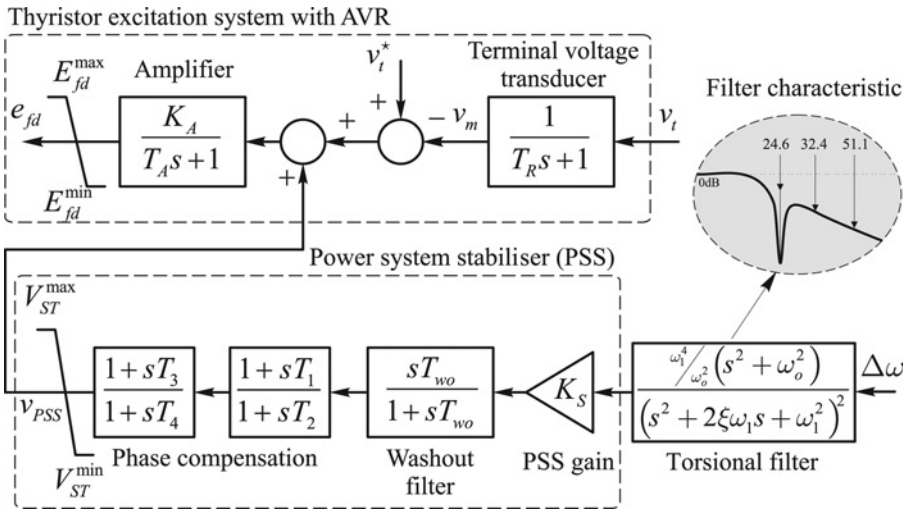

Fig. 2 *Block diagram of the excitation system including AVR, PSS and torsional filter*

(electromagnetic T_e and mechanical T_m), whereas $\boldsymbol{H}$, $\boldsymbol{K}$ and $\boldsymbol{D}$ are the inertia matrix, spring constant matrix, and damping matrix of the multi-mass system, respectively. System (1) and (2) can also be written in a more compact form as

$$\dot{\boldsymbol{x}} = \boldsymbol{A}_{\mathrm{m}}\boldsymbol{x} + \boldsymbol{B}_{\mathrm{m}}\boldsymbol{\tau} \tag{6}$$

where $\boldsymbol{x} \triangleq [\gamma\ \boldsymbol{\omega}]^{\mathrm{T}}$ is a new state vector of the multi-mass system, and $\boldsymbol{\gamma}$ represents the relative angle vector

$$\boldsymbol{\gamma} \triangleq \begin{bmatrix} \gamma_1 & \gamma_2 & \gamma_3 \end{bmatrix}^{\mathrm{T}} = \begin{bmatrix} \theta_1 - \theta_4 & \theta_2 - \theta_4 & \theta_3 - \theta_4 \end{bmatrix}^{\mathrm{T}} \tag{7}$$

2.3 WECS

The variable-speed WECS considered in this work is an aggregated equivalent [37, 38] of a wind power plant based on full converter wind turbines. The electrical machine consists of a permanent magnet generator, the parameters of which are taken from the Siemens wind turbine STW-3.0-101. As shown in several previous works [31, 39, 40], because of electronic converters, the individual powers from each WECS can be controlled in a very fast and precise manner, making it possible to control the total output of the wind farm with a desired target (e.g. SSR mitigation). A two-mass lumped model is used to represent the WECS mechanical dynamics [41, 42]. Other major components are the back-to-back VSCs through which the full power of the wind generator is evacuated to the grid. The machine-side converter is a two-level VSC connected through a filter to the machine stator, whereas the grid-side converter is connected through a step-up transformer and collector line to the grid [1, 42]. The control strategy can be divided into two blocks. On the one hand, the management of the active and reactive powers delivered by the WECS is achieved by the grid-side VSC [39, 43]. On the other hand, the stator current control along with the dc-link voltage regulation are accomplished by the machine-side VSC. The inner current

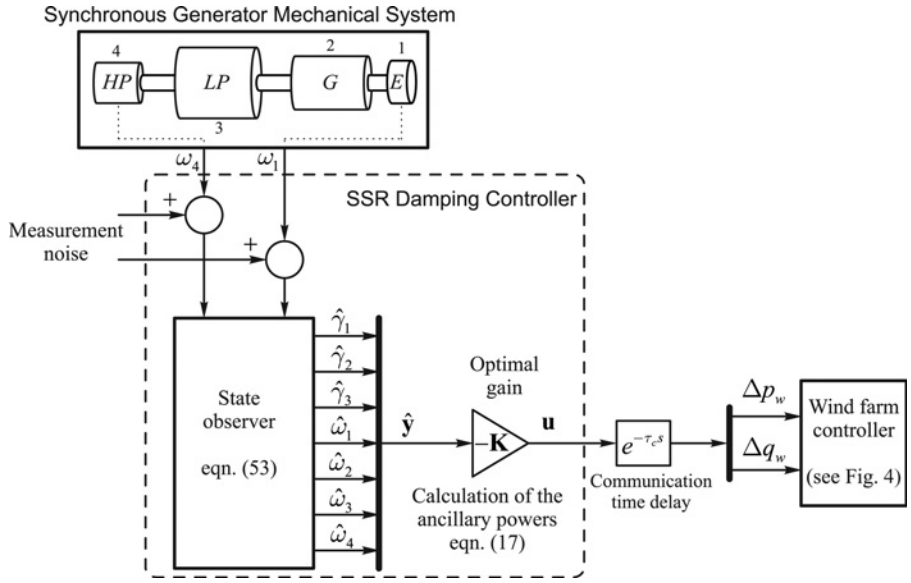

Fig. 3 *Block diagram of the proposed control strategy using speed measurements of the synchronous generator*

control loops of the machine-side VSC and grid-side VSC are implemented using a rotating *dq* control (vector control) aligned with the rotor position and grid voltage space vector, respectively (for further details see [31, 40, 44]). The aerodynamic model, turbine characteristic curve and turbine multi-mass model information are taken from [41–43, 45, 46]. A schematic block diagram of the WECS controller is presented in Fig. 4 and parameters are given in Table 2.

An average model of the VSCs is considered in the small-signal analysis [47]. Dynamic equations, in a per-unit system, of the permanent magnet-based wind generator, the back-to-back converters and the two-mass mechanical

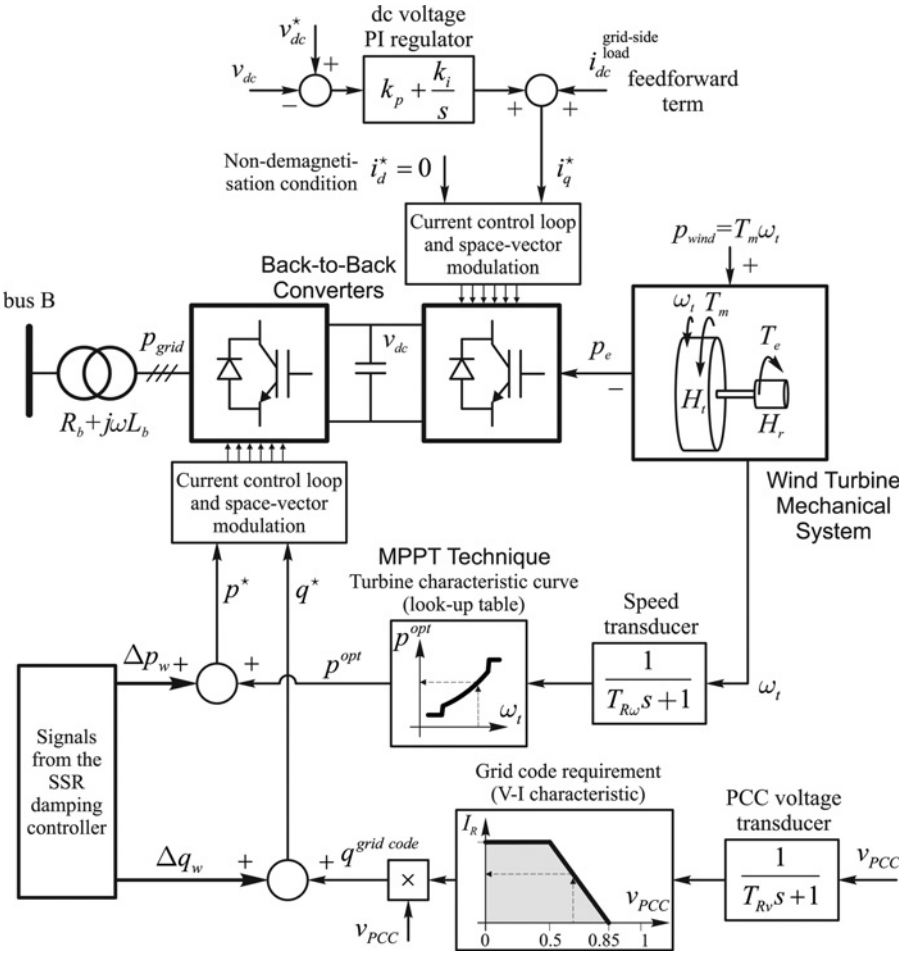

Fig. 4 *Schematic block diagram of the WECS controller*

doi: 10.1049/iet-gtd.2012.0357

Table 2 WECS parameters and data

Description	Symbol	Value
base power (66 × 3 MW SWT-3.0-101)	S_B	200 MVA
low-side base voltage (line-to-line RMS)	V_B	690 V
base frequency (mechanical)	Ω_{Br}	11 RPM
turbine speed range	ω_t	6–16 RPM
DC-link voltage	v_{dc}	1.3 kV
DC-link capacitance	C_{dc}	13 mF
commutation frequency (PWM frequency of VSC)	f_{pwm}	1700 Hz
resistance of turbine step-up transformer	R_b	0.005
inductance of turbine step-up transformer	L_b	0.05
permanent magnet generator flux	Ψ_m	8.15 Wb
generator stator resistance	R_s	0.01
generator stator self-inductance	$L_{sd} = L_{sq}$	0.10
turbine radius	R_t	50.5 m
gearbox ratio (direct drive)	N_{gb}	1
pole-pair number of the generator	N_r	60
wind turbine inertia constant	H_t	3.5 s
generator rotor inertia constant	H_r	0.5 s
equivalent resistance of the 11 kV-line impedance	R_{lv}	0.014
equivalent inductance of the 11 kV-line impedance	L_{lv}	0.14
shaft stiffness	K_{tr}	1079
shaft mutual damping	D_{tr}	19.8
wind turbine mechanical damping	D_t	0.01
electric rotor mechanical damping	D_r	0.01
communication time delay	τ_c	20 ms
proportional gain of the dc-link PI regulator	k_p	0.75
integral gain of the dc-link PI regulator	k_i	3.9
current control loop gain	k_{cc}	900
speed transducer time constant	$T_{R\omega}$	0.017 s
voltage transducer time constant	T_{Rv}	0.02 s
wind speed	v_w	11 m/s
turbine characteristic curve	$P_{opt}(\omega_t)$	from [45]

Except where indicated, parameters are in the per-unit system.

system are given below

$$\frac{L_{sd}}{\Omega_B}\dot{i}_{sd} = -R_s i_{sd} - L_{sq}\omega_r i_{sq} - \eta_{ad} v_{dc} \tag{8}$$

$$\frac{L_{sq}}{\Omega_B}\dot{i}_{sq} = -R_s i_{sq} + L_{sd}\omega_r i_{sd} - \eta_{aq} v_{dc} + \omega_r \Psi_m \tag{9}$$

$$\frac{L_b}{\Omega_B}\dot{i}_{bd} = -R_b i_{bd} - L_b \omega i_{bq} - \eta_{bd} v_{dc} + v_{bd} \tag{10}$$

$$\frac{L_b}{\Omega_B}\dot{i}_{bq} = -R_b i_{bq} + L_b \omega i_{bd} - \eta_{bq} v_{dc} + v_{bq} \tag{11}$$

$$\frac{C_{dc}}{\Omega_B}\dot{v}_{dc} = \frac{3}{2}\left(\eta_{ad} i_{sd} + \eta_{aq} i_{sq} - \eta_{bd} i_{bd} - \eta_{bq} i_{bq}\right) \tag{12}$$

$$2H_t\dot{\omega}_t = T_m - D_t\omega_t - K_{tr}\gamma_{tr} - D_{tr}(\omega_t - \omega_r) \tag{13}$$

$$2H_r\dot{\omega}_r = -T_e - D_r\omega_r + K_{tr}\gamma_{tr} + D_{tr}(\omega_t - \omega_r) \tag{14}$$

$$\dot{\gamma}_{tr} = \Omega_{Br}(\omega_t - \omega_r) \tag{15}$$

where i_{sd} and i_{sq} are the generator stator currents in the dq reference frame; i_{bd} and i_{bq} represent the grid-side VSC currents; v_{bd} and v_{bq} are the dq-axis B-bus voltages; η_{ad}, η_{aq}, η_{bd} and η_{bq} are the duty cycles of the machine- and grid-side converters, respectively. The state variables ω_t, ω_r and γ_{tr} stand for the turbine and rotor speeds and shaft torsional angle (twist angle). The shaft stiffness K_{tr} and shaft mutual damping D_{tr} are related to the inertia constants and mechanical oscillation mode $\lambda = -\xi\omega_n \pm j\omega_n\sqrt{1-\xi^2}$ by $K_{tr} = \left(2H_tH_r\omega_n^2/(H_t + H_r)\Omega_{Br}\right)$ and $D_{tr} = 4H_tH_r\xi\omega_n/(H_t + H_r)$, whereas the electromagnetic torque is given by $T_e = \Psi_m i_{sq} - (L_{sq} - L_{sd})i_{sd}i_{sq}$ (Table 2 presents the rest of the parameter definitions). Grid synchronisation of the WECS grid-side converter is accomplished using the SRF phase-locked loop (SRF-PLL) described in [48, 49].

3 SSR damping controller

Among SSR damping controllers, single-input single-output schemes are widely found in the literature [14–17, 20, 23–28], for instance: PSS-like strategies [14, 17, 26], variants of proportional–integral–derivative (PID) structures [15, 23, 27, 28] and controllers based on proportional plus high-pass filters [16, 20, 24]. Since we are intended to control the active and reactive powers of the WECS, and because it allows an easier control tuning when several measurement channels and control inputs are involved, a multi-input–multi-output (MIMO) approach is chosen to design the SSR damping controller.

The power system under study has more than 30 state variables. To design a controller with such a high order model is neither practical nor necessary. Therefore model reduction is often applied to obtain a lower order model for the control design stage [13, 19, 50, 51]. The following representation of the reduced system model is obtained by using the procedure introduced in Appendix 1

$$\dot{\boldsymbol{y}} = \boldsymbol{T}\boldsymbol{S}_L^T\boldsymbol{A}\boldsymbol{S}_R\boldsymbol{T}^{-1}\boldsymbol{y} + \boldsymbol{T}\boldsymbol{S}_L^T\boldsymbol{B}\boldsymbol{u} \tag{16}$$

where the vector $\boldsymbol{y}$ represents the measurements to be fed back; $\boldsymbol{S}_L$ and $\boldsymbol{S}_R$ are matrices which allow us to reduce the power system model, and $\boldsymbol{u} = [\Delta p_w \ \Delta q_w]^T$ is the vector, which contains the control inputs from the SSR damping controller (further details of the derivation of (16) are developed in Appendices 1 and 2). These supplementary signals $\boldsymbol{u}$ are additional active and reactive powers injected by the WECS (see Fig. 4 to see how these signals enter the WECS control).

With the obtained system (16), it is possible to apply MIMO state-feedback control strategies. Therefore the control signal $\boldsymbol{u}$ can be obtained as

$$\boldsymbol{u} = -\boldsymbol{K}\boldsymbol{y} \tag{17}$$

where $\boldsymbol{K}$ is the control gain matrix. To maximise the oscillation damping and minimise the control efforts, the control gain $\boldsymbol{K}$ is calculated based on an optimal quadratic technique [52]. The optimal control gain is obtained by minimising the cost function $J = \int(\boldsymbol{y}^T\boldsymbol{Q}\boldsymbol{y} + \boldsymbol{u}^T\boldsymbol{R}\boldsymbol{u})\,dt$. This index can be built to weigh both output deviations $\boldsymbol{y}$ and control inputs $\boldsymbol{u}$ through the design matrices $\boldsymbol{Q}$ and $\boldsymbol{R}$ [53].

4 Measurement selection

4.1 Optimal measurements

Several techniques to select the best states to be fed back can be found in the literature. We choose the method based on participation factors, as it does not undergo scaling problems when there are measurements of a different physical significance [54]. The participation factor gives a

dimensionless measure of the association between the ith mode and the kth state [34]. In the SSR phenomenon, the modes of interest are the mechanical torsional ones. The above method reveals that angles and speeds of the multi-mass system have the higher participation factors of torsional modes. Consequently, these states can be chosen to build the measurement vector $\boldsymbol{y}$, yielding

$$\boldsymbol{y} = \begin{bmatrix} \gamma_1 & \gamma_2 & \gamma_3 & \omega_1 - \omega_4 & \omega_2 - \omega_4 & \omega_3 - \omega_4 \end{bmatrix}^{\mathrm{T}} \quad (18)$$

Note that relative angles and relative speeds are considered. In this way, the damping controller is only focused on the shaft torsional oscillations and does not act on the electromechanical mode. This allows WECS control efforts to be maximised to reduce SSR, whereas the PSS damps electromechanical oscillations. It is also important to remark that the SSR damping controller only works when relative speed deviations are detected in the shaft. Therefore under normal operating conditions, the WECSs accomplish their typical tasks to fulfill the grid code requirements and to follow the maximum power point tracking (MPPT) algorithm [55] (being in steady state $\Delta p_w = \Delta q_w \cong 0$). Fig. 3 presents a general block diagram showing the implementation of the proposed SSR damping controller using mechanical measurements of the synchronous generator.

The control law calculated with the measurement vector (18) requires the measurement of relative angles (γ_1, γ_2, γ_3) and angular speeds (ω_1, ω_2, ω_3, ω_4). In order to reduce the amount of sensors and to avoid imprecise or unavailable measurements, a state observer is implemented to properly estimate the necessary measurements [56, 57]. The observer measures a pair of speeds (ω_1, ω_4) and uses the multi-mass system model to estimate the rest of the states (γ_1, γ_2, γ_3, ω_2, ω_3). The full derivation of the state observer is developed in Appendix 3. An additional advantage is also provided by the observer since its filter action reduces measurement noises.

4.2 Communication time delays

For the SSR damping control, the required measurements should arrive through a fast communication system (e.g. optical fibre). This is possible with current communication links (such as PROFIBUS, EtherCAT etc.) along with the recent progress in digital fibre-optic communication systems and real-time control computers, which have shown a latency of less than 26 ms (see [58], as well as [20, 23] where remote speed measurements were also used to damp SSR oscillations). These time delays can even be reduced considering the distances of this particular application and the advances in current communication systems. In case this requirement is fulfilled, the possible time delays do not affect the proposed control strategy performance. If the latency is longer, a phase compensator can be used, such as those based on lead lag filters [19, 59, 60], Padé approximations [51, 61], Smith predictor [62–64] or phase-shift techniques [65]. Time delays longer than 50 ms have to be avoided since the required control bandwidth could not be enough to damp the SSR oscillations, as mentioned in [23, 24].

In the case of very large wind farms where such fast communication protocols cannot be applied for all wind turbines, only those turbines near the synchronous generator should be considered for the SSR mitigation. That is in wind farms with turbines placed on a large geographical area, it is considered the group of machines closer to the synchronous generator which can reach a power ratio of 1:3 or 1:4 to properly accomplish the SSR mitigation. Section 5 shows that the SSR mitigation can be accomplished in about 3 s with a power ratio of 1:3 between the wind farm and the synchronous generator. However, if we allow a slower SSR damping lasting about 4 or 5 s, which still carries out a good system performance, the power ratio can be reduced to 1:4 or 1:5, consequently diminishing both the required wind farm size and geographical extension, and then reducing the time-delays.

4.3 Local measurements

As an alternative to measure the synchronous generator mechanical speed, a local set of measurements is chosen to avoid the communication link between the synchronous generator facility and the wind farm. This can be accomplished by using the voltage measurement at the wind farm point of common coupling (PCC), $\boldsymbol{y} = [v_d^{\mathrm{PCC}} \; v_q^{\mathrm{PCC}}]^{\mathrm{T}}$. Although this voltage does not have the high observability index of the torsional modes as the synchronous generator mechanical speeds, it can also be used to reduce the SSR oscillations as shown in [25]. In this way, two control schemes using remote and local measurements are compared and advantages and disadvantages of both schemes will be presented in the next section.

5 Performance testing

This section presents the most relevant results regarding the assessment of the proposed SSR damping controllers. Power system tests were performed using the most detailed electromagnetic transient (EMT) models from SimPowerSystems blockset of SIMULINK/MATLAB®. Time-domain simulations take into account a wide range of phenomena, from insulated gate bipolar transistor (IGBT) switching to mechanical dynamics. The power system configuration is shown in Fig. 1. Power system and variable-speed WECS parameters are given in Tables 1 and 2.

There are two types of SSR problems: first, the steady-state SSR (induction generator effect (IGE) and torsional interaction (TI)); second, the transient SSR (shaft torque amplification (TA)) [8]. IGE and TI phenomena have to be analysed by using small-signal or eigenvalue tools, since they can involve slowly growing oscillations, which could be difficult to identify with time-domain programs. On the other hand, TA phenomenon has to be studied by using non-linear time-domain simulations, since large disturbances and transient variations of non-linear variables are expected [7].

5.1 Eigenvalue analysis

Fig. 5*a* shows the variation of the imaginary part of eigenvalues with respect to the percentage of series compensation. It can be seen that, while series-compensation level varies, the imaginary part of the first, second and third torsional modes and the electromechanical mode remains without appreciable changes. On the other hand, there are two modes which start to separate from each other; they represent the electrical network modes described in the rotating coordinates. The increasing mode is called supersynchronous and the decreasing mode is called

doi: 10.1049/iet-gtd.2012.0357

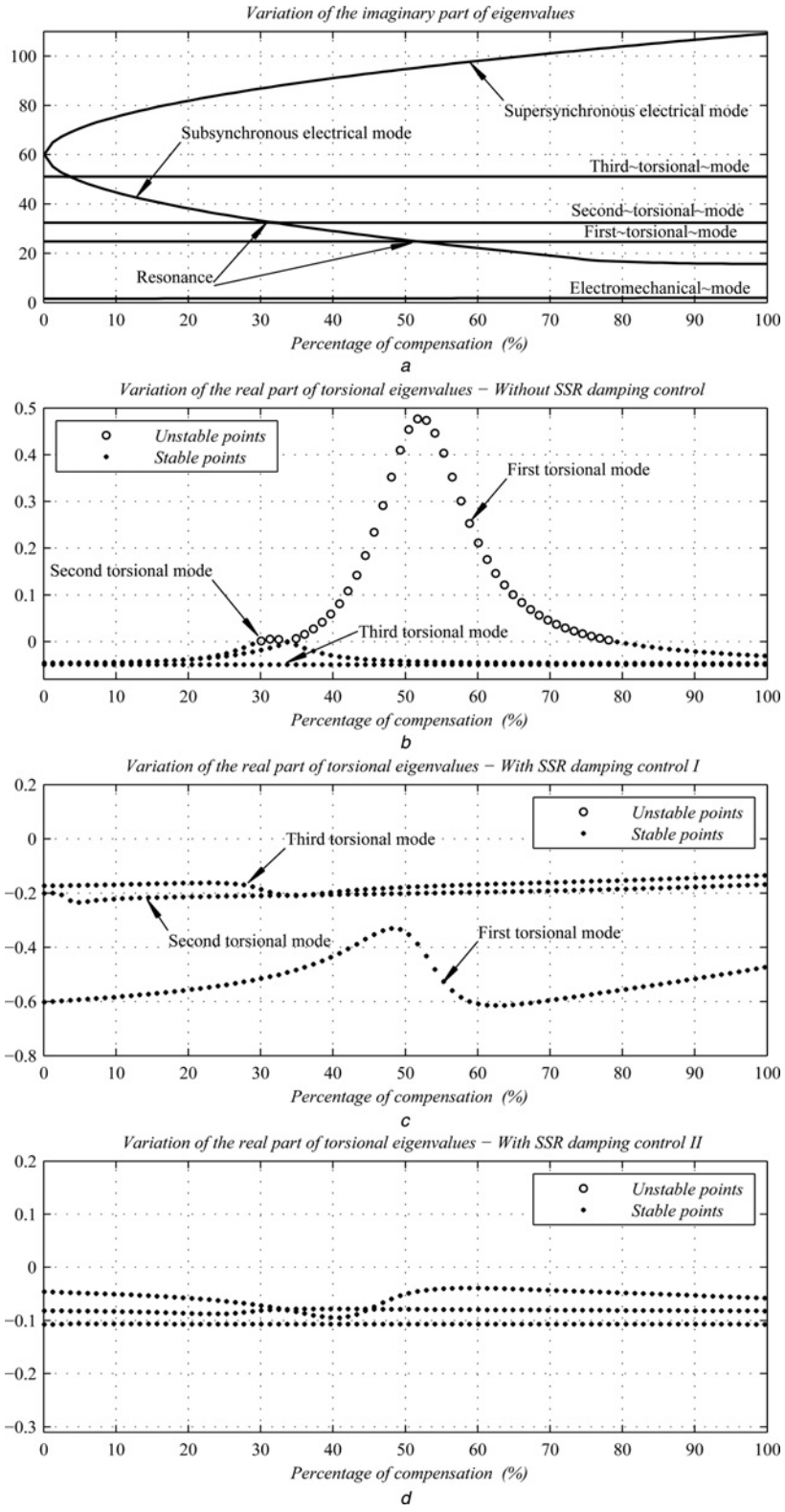

Fig. 5 *Variation of the real and imaginary parts of main eigenvalues with respect to the percentage of series compensation*

a Variation of the imaginary part of eigenvalues
b Variation of the real part of torsional eigenvalues – without SSR damping control
c Variation of the real part of torsional eigenvalues – with SSR damping control I
d Variation of the real part of torsional eigenvalues – with SSR damping control II

subsynchronous. When the last one falls, it interacts with the shaft torsional modes causing the SSR phenomenon [66].

Fig. 5*b* shows the variation of the real part of the three torsional eigenvalues without an SSR damping control. There are certain compensation levels in which the real part is positive (see circled points in Fig. 5*b*). Therefore the system will be unstable and shaft damage can be caused, if the generator is not tripped. On the contrary, when the

Table 3 Small-signal analysis

	Without SSR damping control		With SSR damping control I		With SSR damping control II	
	f_n, Hz	ζ, %	f_n, Hz	ζ, %	f_n, Hz	ζ, %
Without series-compensation						
first torsional mode	24.71	*0.031*	24.72	**0.388**	24.82	**0.040**
second torsional mode	32.38	*0.022*	32.39	**0.086**	32.39	**0.039**
third torsional mode	51.11	*0.015*	51.11	**0.063**	51.11	**0.033**
electromechanical mode	1.635	28.86	1.635	28.80	2.171	38.42
subsynchronous mode	60.00	1.035	60.01	1.031	60.00	1.102
supersynchronous mode	60.04	4.395	60.03	4.352	60.02	5.781
25% Series-compensation						
first torsional mode	24.72	*0.020*	24.72	**0.348**	24.83	**0.042**
second torsional mode	32.38	*0.013*	32.39	**0.081**	32.40	**0.044**
third torsional mode	51.11	*0.015*	51.11	**0.066**	51.11	**0.033**
electromechanical mode	1.700	30.34	1.700	30.29	2.184	38.31
subsynchronous mode	35.64	6.829	35.65	6.835	33.87	9.583
supersynchronous mode	84.47	2.933	84.47	2.927	86.32	3.749
50% Series-compensation						
first torsional mode	24.73	*−0.281*	24.69	**0.222**	24.84	**0.033**
second torsional mode	32.38	*0.021*	32.39	**0.088**	32.40	**0.040**
third torsional mode	51.11	*0.015*	51.11	**0.063**	51.11	**0.033**
electromechanical mode	1.792	32.62	1.793	32.57	2.202	38.14
subsynchronous mode	25.46	9.718	25.50	9.526	22.81	14.40
supersynchronous mode	94.69	2.621	94.68	2.617	97.47	3.358
75% Series-compensation						
first torsional mode	24.68	*−0.009*	24.72	**0.372**	24.84	**0.029**
second torsional mode	32.38	*0.023*	32.39	**0.077**	32.40	**0.040**
third torsional mode	51.11	*0.015*	51.11	**0.059**	51.11	**0.033**
electromechanical mode	1.937	36.60	1.938	36.56	2.225	37.85
subsynchronous mode	17.60	15.25	17.58	15.23	14.44	22.70
supersynchronous mode	102.5	2.423	102.5	2.412	106.0	3.101

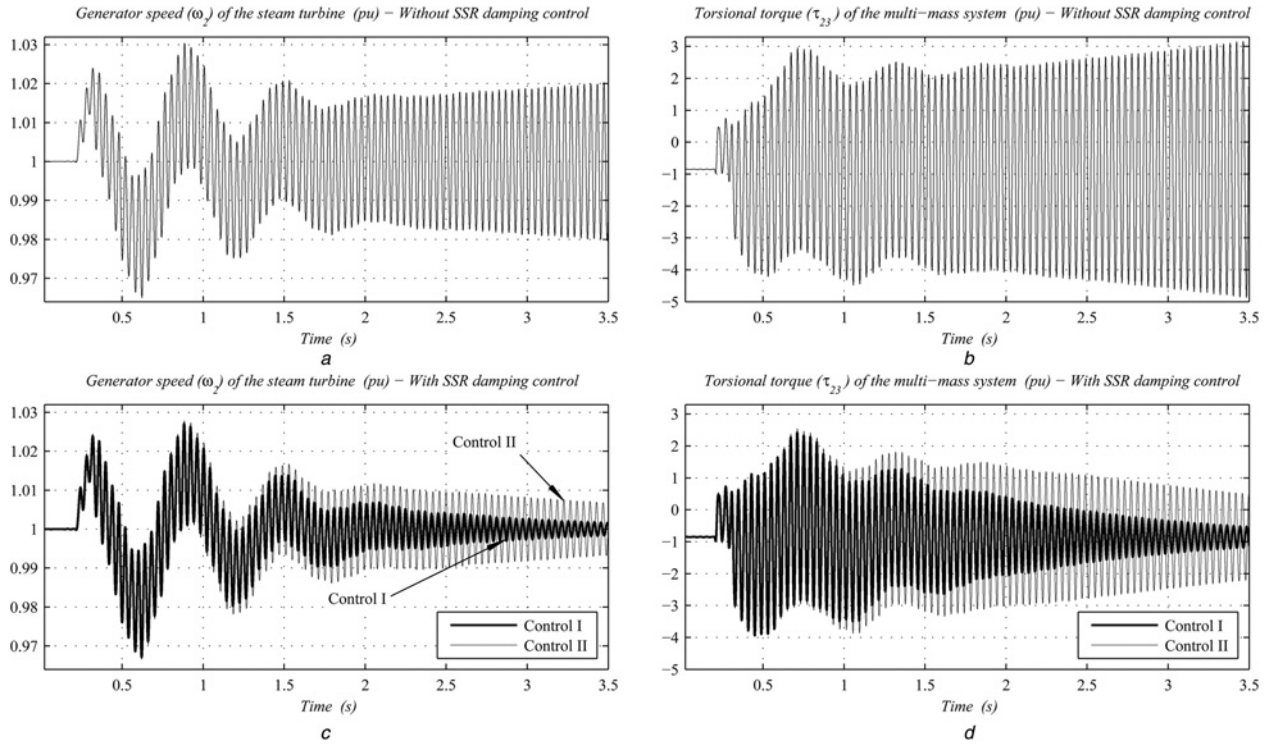

Fig. 6 *System transient response against a 100 ms three-phase fault at the B1-bus, without and with the SSR damping controller*

a Generator speed of the steam turbine – without SSR damping control
b Generator/low presssure turbine torsional torque – without SSR damping control
c Generator speed of the steam turbine – with SSR damping control
d Generator/low-pressure turbine torsional torque – with SSR damping control

doi: 10.1049/iet-gtd.2012.0357

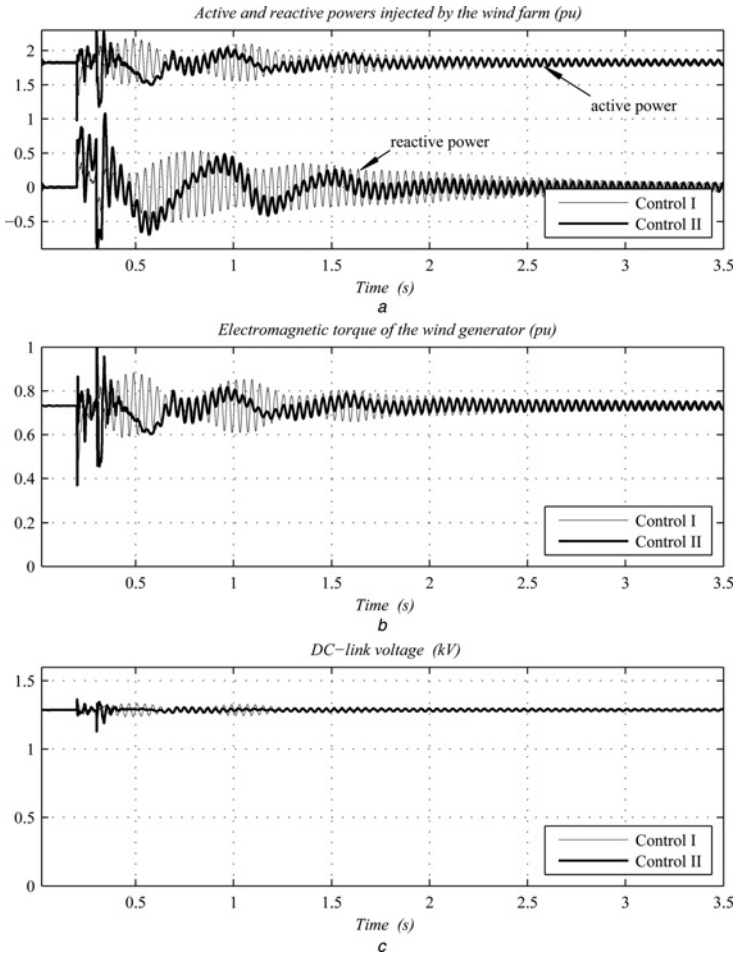

Fig. 7 *Internal variables of the wind farm while performing the SSR damping task*

a Active and reactive poweres injected by the wind farm
b Electromagnetic torque of the wind generator
c DC-link voltage

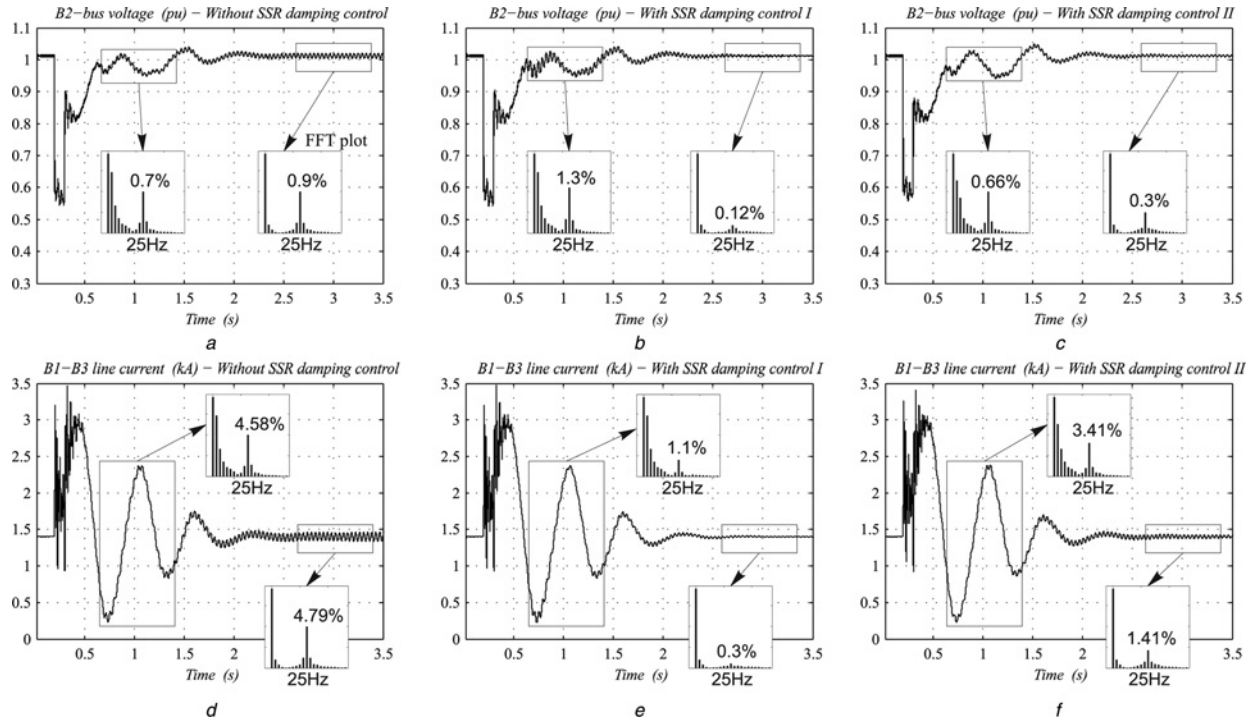

Fig. 8 *Waveforms and FFT plots of the B2-bus voltage and B1–B3 line current*

a–c B2-bus voltage with and without the SSR damping control
d–f B1-B3 line current with and without the SSR damping control

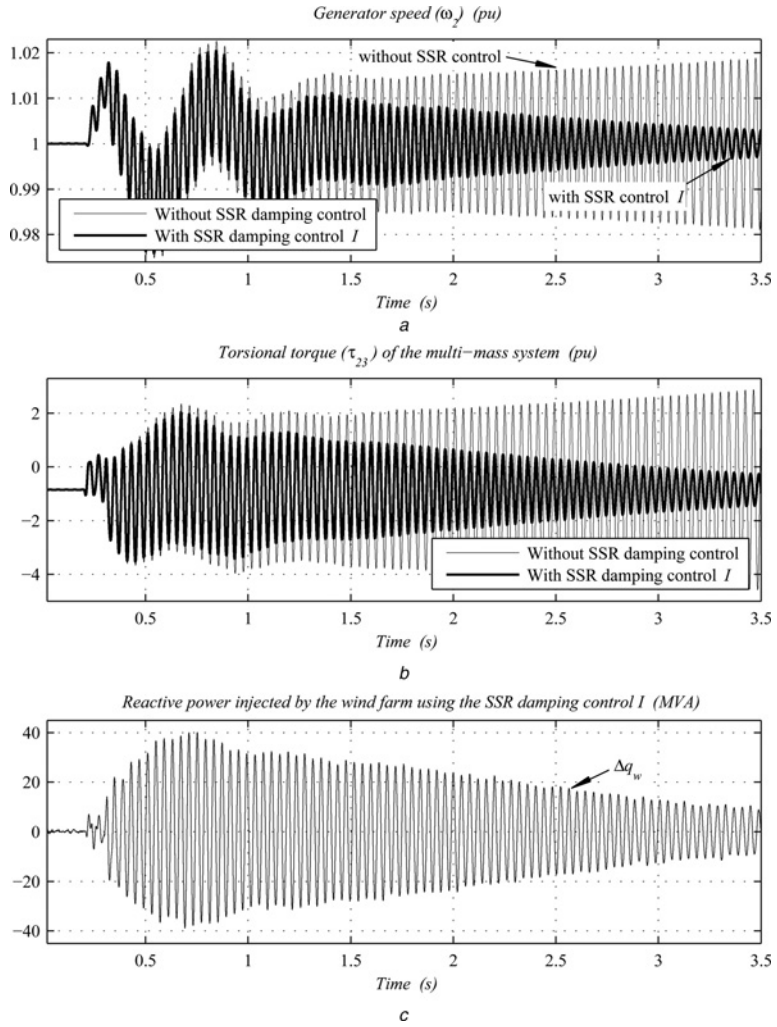

Fig. 9 *Speed and torque oscillation damping improvement at zero active power production of the WECS*

a Generator speed
b Generator/low-pressure turbine torsional torque
c Reactive power injected by the wind farm using the SSR damping control I

proposed SSR damping controllers are added to the WECS, the real part is always negative, irrespectively of the series-compensation level (see Figs. 5*c* and *d*). In order to compare both controllers, we tune their control gains to obtain approximately the same control efforts (ancillary powers injected by the WECS to the grid). It can also be observed that the controller measuring the synchronous generator mechanical speed (called control I, Fig. 5*c*) achieves a bigger negative real part of the torsional modes than the controller measuring the PCC voltage (called control II, Fig. 5*d*), which implies that the control I can better damp the torsional oscillations for the same control effort.

The frequency f_n and damping ratios ζ of the main oscillatory modes are illustrated in Table 3. The damping ratios of the three torsional modes without an SSR damping control are approximately improved by four times when using the control I, and two times when using the control II (see in Table 3, the damping ratios in italics font against damping ratios in bold font).

5.2 Non-linear time-domain simulations

5.2.1 Transient response and damping injection: A three-phase fault is introduced at the B1-bus (see Fig. 1) in order to evaluate the system transient response. We analyse an operating point where the synchronous generator is delivering 510 MW, and the wind farm 190 MW. A 50% of series compensation is considered since, from a torsional mode damping point of view, it is one of the worst cases (see Table 3). Figs. 6*a* and *c* show the generator speed (ω_2), and the generator/low-pressure turbine torsional torque (τ_{23}) is presented in Figs. 6*b* and *d*. By comparing Figs. 6*a* and 6*b* (without SSR damping controller) with Figs. 6*c* and *d* (with SSR damping controller), it is clear the improvement of both the speed and torsional torque damping when the WECS-based SSR damping controller is implemented. Figs. 6*c* and *d* show with thick line the control scheme I and with thin line the control scheme II, where, as expected, a larger oscillation damping capacity is accomplished by the control I in agreement with the results obtained in the previous subsection.

In order to assess the impact of the supplementary SSR damping task on the WECS, Fig. 7 shows several internal variables of the wind farm (thin line for the control I and thick line for the control II). Active and reactive powers delivered by the WECS are presented in Fig. 7*a*, where power variations lesser than ±50 MVA (25% of WECS capacity) are only needed to achieve the SSR damping. The electromagnetic torque of the wind generator is illustrated in Fig. 7*b*; there are variations smaller than 15% of the

doi: 10.1049/iet-gtd.2012.0357

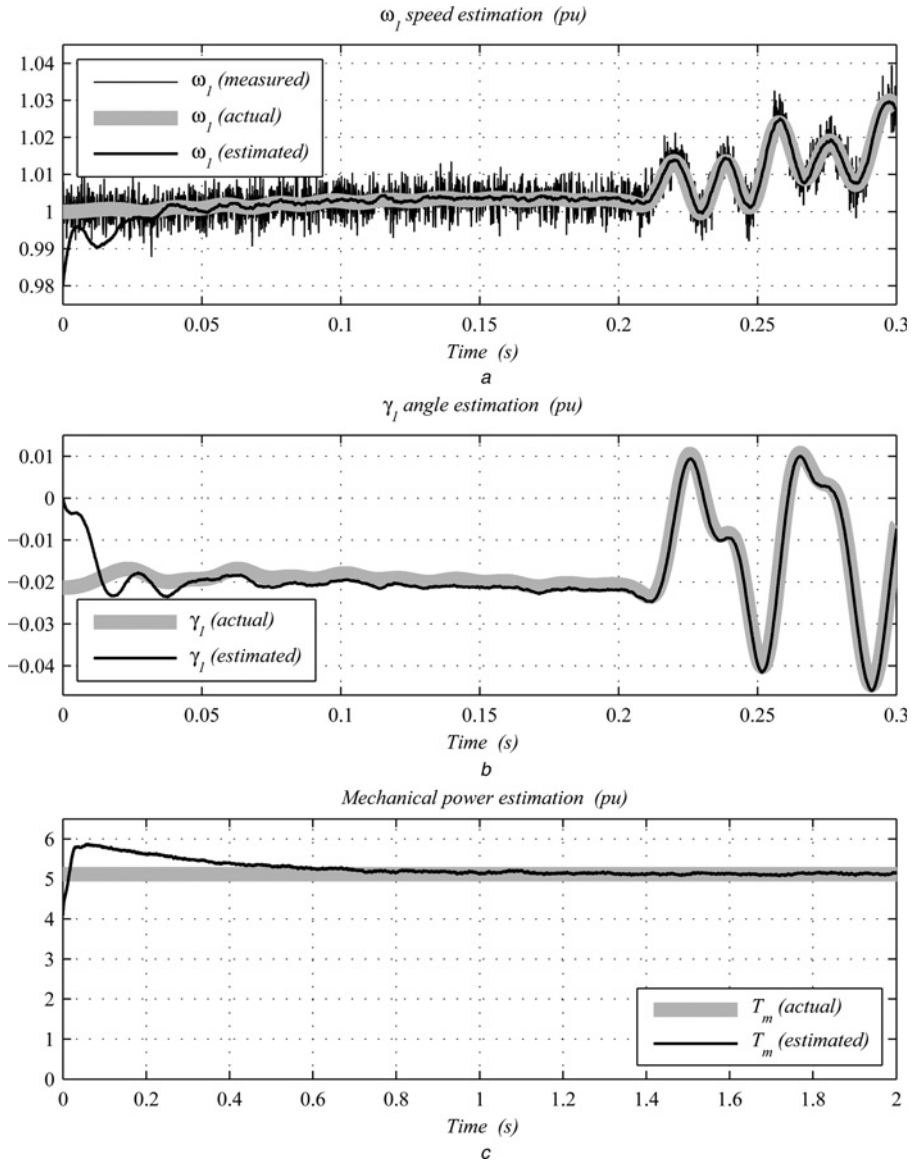

Fig. 10 *State observer convergence*

Actual values (thick line) and estimated values (thin line)
a Speed estimation
b Angle estimation
c Mechanical power estimation

nominal torque, which are lower than the transient peak produced at the fault instant. Then, Fig. 7*c* presents the dc-link voltage regulation which allows the dc voltage to remain inside of the normal operating range.

Although it is not shown because of space reasons, we studied other operating points where the wind farm is delivering 33% of its nominal capacity, and the synchronous generator is generating 40% of its rated power. In all these tests both torsional mode damping improvement and good operation of the wind farm were also attained.

5.2.2 Impact on the power quality of the grid: As the wind farm injects an additional active and reactive power to the grid, the B2-bus voltage and B1–B3 line current will be analysed. Fig. 8 shows their waveforms and fast Fourier transform (FFT) plots at different time intervals (immediately after the fault and at steady state). These results along with harmonic spectrum are used to compare and evaluate three cases: without SSR control (Figs. 8*a* and *d*), with remote SSR control (control I, Figs. 8*b* and *e*), and with local SSR control (control II, Figs. 8*c* and *f*).

A dominant frequency of approximately 25 Hz is observed for all waveforms because the chosen series compensation level is exciting the first torsional mode of the synchronous generator mechanical system. Immediately after the fault, the control I increases the 25 Hz harmonic in the B2-bus voltage since the WECS converter is injecting reactive power to reduce the SSR oscillation. However, this harmonic increment is only produced transiently for a short period of time, and it is a small price to pay to mitigate the SSR oscillations. On the other hand, the 25 Hz harmonic is highly reduced in both voltage and current waveforms after 3 s of the fault event, when controllers I and II are implemented. As a conclusion, we can say that SSR subharmonics are reduced when the proposed controllers are considered, having the control I a better performance than the control II, except for a small transient increment in the voltage in the control I case.

5.2.3 SSR oscillation damping in no wind conditions: The grid-side converter of a wind turbine can be synchronised and connected to the grid, even though when the wind is not enough to generate active power [67]. In situations of no wind, this converter can be used as a STATCOM (injecting reactive power) to accomplish network support tasks like voltage regulation and, in our case, to perform the SSR mitigation. Therefore to evaluate the control performance under this condition, we made a similar test of Section 5.2.1 but at zero active power production of the WECS. Figs. 9*a* and *b* show the SSR oscillations in the generator speed ω_2 and torsional torque τ_{23} after the fault event, and cases with and without SSR damping control are presented (for clarity, only the control I is shown). It can be observed that the oscillations are reduced when the grid-side converter injects the reactive power component Δq_w calculated by the SSR damping controller (see Fig. 9*c*).

5.2.4 Assessment of the state estimation: Finally, the state observer performance is illustrated in Fig. 10. Fig. 10*a* shows the initial convergence and the noise attenuation of the measurement ω_1. Figs. 10*b* and *c* show the relative angle γ_1 and mechanical power estimates when an erroneous initial condition is given to the observer. In all cases, a fast, accurate, and noise-free convergence to the actual states is accomplished.

6 Conclusions

In this work, we investigated the ability to reduce the risk of SSR oscillations using variable-speed WECSs based on full converter wind turbines. It was found that significant torsional oscillation damping could be accomplished when appropriate supplementary powers are transiently delivered by the WECS located near thermal power plants.

At the project stage, when studying whether to include a series compensation or to increase the current series compensation level, instead of only considering the traditional methods to damp SSR oscillations (which can result in additional costs), it can also be analysed the possibility to damp those SSR oscillations using the converters of near wind farms. In this way, we can use already installed facilities and reduce costs. It is important that the wind farm is in the vicinity of the synchronous generator in order to the WECS converters have controllability over its torsional modes. If the wind farm is far from the synchronous generator, it could not have enough controllability and observability and another classical local SSR mitigation mechanism has to be explored.

Performance comparisons of two control approaches using remote and local measurements were analysed: the first one uses mechanical measurements of the synchronous generator (measures which have high observability of torsional modes), and the second one uses voltage measurements at the PCC (avoiding the communication link between the synchronous generator and the wind farm). We discussed power ratio between the wind farm and the synchronous generator, impact on the power quality, and communication time-delay requirements. A test was also introduced to demonstrate the SSR damping capability when there is no sufficient wind to generate active power; therefore using the grid-side converter as a STATCOM device.

Features such as speed and stored energy are naturally found in WECSs, which can resort to their stored kinetic energy through power electronics and, at the same time, inject reactive power. These characteristics give the WECS-based SSR mitigation an advantage against traditional approaches based on FACTS. Moreover, the new wind farms installed in the grid make possible this kind of SSR mitigation without the inclusion of expensive dedicated SSR damping equipment.

Eigenvalue analysis and non-linear time-domain tests showed that the SSR damping strategy can provide satisfactory torsional damping under a wide variation of series-compensation levels.

7 Acknowledgments

This work was supported in part by Universidad Nacional del Sur (UNS), Consejo Nacional de Investigaciones Científicas y Técnicas (CONICET) and Agencia Nacional de Promoción Científica y Tecnológica (ANPCyT), Argentina, and in part by the Spanish Ministry of Education and Science (MEC) and Junta de Andalucía under grants ENE2011-24137 and P09-TEP-5170, respectively.

8 References

1 Liserre, M., Cardenas, R., Molinas, M., Rodriguez, J.: 'Overview of multi-MW wind turbines and wind parks', *IEEE Trans. Ind. Electron.*, 2011, **58**, (4), pp. 1081–1095
2 Hughes, F.M., Anaya-Lara, O., Jenkins, N., Strbac, G.: 'Control of DFIG-based wind generation for power network support', *IEEE Trans. Power Syst.*, 2005, **20**, (4), pp. 1958–1966
3 Tapia, G., Tapia, A., Ostolaza, J.X.: 'Proportional-integral regulator-based approach to wind farm reactive power management for secondary voltage control', *IEEE Trans. Energy Convers.*, 2007, **22**, (2), pp. 488–498
4 Anaya-Lara, O., Hughes, F.M., Jenkins, N., Strbac, G.: 'Contribution of DFIG-based wind farms to power system short-term frequency regulation', *IEE Proc. Gener., Transm. Distrib.*, 2006, **153**, (2), pp. 164–170
5 Mauricio, J.M., Marano, A., Gomez-Exposito, A., Martinez Ramos, J.L.: 'Frequency regulation contribution through variable-speed wind energy conversion systems', *IEEE Trans. Power Syst.*, 2009, **24**, (1), pp. 173–180
6 Yang, L., Yang, G.Y., Xu, Z., Dong, Z.Y., Wong, K.P., Ma, X.: 'Optimal controller design of a doubly-fed induction generator wind turbine system for small signal stability enhancement', *IET Gener., Transm. Distrib.*, 2010, **4**, (5), pp. 579–597
7 IEEE Committee Report: 'Reader's guide to subsynchronous resonance', *IEEE Trans. Power Syst.*, 1992, **7**, (1), pp. 150–157
8 Anderson, P.M., Agrawal, B.L., Van Ness, J.E.: 'Subsynchronous resonance in power systems' (IEEE Press, Piscataway, New York, 1990)
9 Butler, J.W., Concordia, C.: 'Analysis of series capacitor application problems', *AIEE Trans.*, 1937, **56**, (8), pp. 975–988
10 Walker, D.N., Bowler, C.E.J., Jackson, R.L., Hodges, D.A.: 'Results of subsynchronous resonance test at Mohave', *IEEE Trans. Power Appar Syst.*, 1975, **94**, (5), pp. 1878–1889
11 Hingorani, N.G., Gyugyi, L.: 'Understanding FACTS: concepts and technology of flexible AC transmission system' (IEEE Press, 1999)
12 Rai, D., Faried, S.O., Ramakrishna, G., Edris, A.: 'Hybrid series compensation scheme capable of damping subsynchronous resonance', *IET Gener., Transm. Distrib.*, 2001, **4**, (3), pp. 456–466
13 Wang, L., Huang, C.-W.: 'Suppression of subsynchronous resonance using robust H∞ TCSC damping controllers'. IEEE Power Engineering Society Winter Meeting, February 1999, vol. 1, pp. 610–615
14 Joshi, S.R., Cheriyan, E.P., Kulkarni, A.M.: 'Output feedback SSR damping controller design based on modular discrete-time dynamic model of TCSC', *IET Gener., Transm. Distrib.*, 2009, **3**, (6), pp. 561–573
15 Pilotto, L.A.S., Bianco, A., Long, W.F., Edris, A.-A.: 'Impact of TCSC control methodologies on subsynchronous oscillations', *IEEE Trans. Power Del.*, 2003, **18**, (1), pp. 243–252
16 de Jesus, F.D., Watanabe, E.H., de Souza, L.F.W., Alves, J.E.R.: 'SSR and power oscillation damping using gate-controlled series capacitors (GCSC)', *IEEE Trans. Power Del.*, 2007, **22**, (3), pp. 1806–1812

doi: 10.1049/iet-gtd.2012.0357

17 Jowder, F.A.R.A., Ooi, B.-T.: 'Series compensation of radial power system by a combination of SSSC and dielectric capacitors', *IEEE Trans. Power Del.*, 2005, **20**, (1), pp. 458–465
18 Bongiorno, M., Angquist, L., Svensson, J.: 'A novel control strategy for subsynchronous resonance mitigation using SSSC', *IEEE Trans. Power Del.*, 2008, **23**, (2), pp. 1033–1041
19 Pillai, G.N., Ghosh, A., Joshi, A.: 'Robust control of SSSC to improve torsional damping'. IEEE Power Engineering Society Winter Meeting, 2001, vol. 3, pp. 1115–1120
20 Farahani, M.: 'Damping of subsynchronous oscillations in power system using static synchronous series compensator', *IET Gener., Transm. Distrib.*, 2012, **6**, (6), pp. 539–544
21 Lee, S., Liu, C.-C.: 'Damping torsional oscillations using a SIMO static VAR controller', *IEE Proc. Gener., Transm. Distrib.*, 1993, **140**, (6), pp. 462–468
22 Hsu, Y.-Y., Jeng, L.-H.: 'Damping of subsynchronous oscillations using adaptive controllers tuned by artificial neural networks', *IEE Proc. Gener., Transm. Distrib.*, 1995, **142**, (4), pp. 415–422
23 Varma, R.K., Auddy, S.: 'Mitigation of subsynchronous resonance by SVC using PMU-acquired remote generator speed'. IEEE Power India Conf., 2006, pp. 1–8
24 Salemnia, A., Khederzadeh, M., Ghorbani, A.: 'Mitigation of subsynchronous oscillations by 48-pulse VSC STATCOM using remote signal', *IEEE PowerTech.*, 2009, **1**, pp. 1–7
25 Padiyar, K.R., Prabhu, N.: 'Design and performance evaluation of subsynchronous damping controller with STATCOM', *IEEE Trans. Power Del.*, 2006, **21**, (3), pp. 1398–1405
26 Keshavan, B.K., Prabhu, N.: 'Damping of subsynchronous oscillations using STATCOM – A FACTS controller'. Int. Conf. on Power System Tech., PowerCon'04, November 2004, vol. 1, pp. 12–16
27 Wang, L., Lee, S.-M., Huang, C.-L.: 'Damping subsynchronous resonance using superconducting magnetic energy storage unit', *IEEE Trans. Energy Convers.*, 1994, **9**, (4), pp. 770–777
28 Fischer de Toledo, P., Angquist, L., Nee, H.-P.: 'Frequency-domain modelling of sub-synchronous torsional interaction of synchronous machines and a high voltage direct current transmission link with line-commutated converters', *IET Gener., Transm. Distrib.*, 2010, **4**, (3), pp. 418–431
29 Bo, W., Yan, Z.: 'Damping subsynchronous oscillation using UPFC. A FACTS device'. Proc. Inter. Conf. on Power System Tech., PowerCon'02, October 2002, vol. 4, pp. 2298–2301
30 Padiyar, K.R., Prabhu, N.: 'Analysis of SSR with three-level twelve-pulse VSC-based interline power-flow controller', *IEEE Trans. Power Del.*, 2007, **22**, (3), pp. 1688–1695
31 Chinchilla, M., Arnaltes, S., Burgos, J.C.: 'Control of permanent-magnet generators applied to variable-speed wind-energy systems connected to the grid', *IEEE Trans. Energy Convers.*, 2006, **21**, (1), pp. 130–135
32 Leon, A.E., Mauricio, J.M., Solsona, J.A.: 'Fault ride-through enhancement of DFIG-based wind generation considering unbalanced and distorted conditions', *IEEE Trans. Energy Convers.*, 2012, **27**, (3), pp. 775–783
33 IEEE SSR Task Force: 'Second benchmark model for computer simulation of subsynchronous resonance', *IEEE Trans. Power Appar. Syst.*, 1985, **104**, (5), pp. 1057–1066
34 Kundur, P.: 'Power system stability and control' (McGraw-Hill, New York, 1994)
35 Watson, W., Coultes, M.E.: 'Static exciter stabilizing signals on large generators – mechanical problems', *IEEE Trans. Power Appar. Syst.*, 1973, **92**, (1), pp. 204–211
36 Lin, W.M., Tsai, C.C., Lin, C.H.: 'Analysing the linear equivalent circuits of electromechanical systems for steam turbine generator units', *IET Gener., Transm. Distrib.*, 2011, **5**, (7), pp. 685–693
37 Akhmatov, V., Knudsen, H.: 'An aggregate model of a grid-connected, large-scale, offshore wind farm for power stability investigations-importance of windmill mechanical system', *Int. J. Electr. Power Energy Syst.*, 2002, **24**, (9), pp. 709–717
38 Trudnowski, D.J., Gentile, A., Khan, J.M., Petritz, E.M.: 'Fixed-speed wind-generator and wind-park modeling for transient stability studies', *IEEE Trans. Power Syst.*, 2004, **19**, (4), pp. 1911–1917
39 Nelson, R.J., Ma, H., Goldenbaum, N.M.: 'Fault ride-through capabilities of siemens full-converter wind turbines'. IEEE Power and Energy Society General Meeting, July 2011, pp. 1–5
40 Leon, A.E., Mauricio, J.M., Gomez-Exposito, A., Solsona, J.A.: 'An improved control strategy for hybrid wind farms', *IEEE Trans. Sust. Energy*, 2010, **1**, (3), pp. 131–141
41 Muyeen, S.M., Ali, M.H., Takahashi, R., *et al.*: 'Comparative study on transient stability analysis of wind turbine generator system using different drive train models', *IET Renew. Power Gener.*, 2007, **1**, (2), pp. 131–141
42 Ellis, A., Kazachkov, Y., Muljadi, E., Pourbeik, P., Sanchez-Gasca, J.J.: 'Description and technical specifications for generic WTG models – A status report'. IEEE/PES Power Systems Conf. and Exposition, March 2011, pp. 1–8
43 Nanou, S., Tsourakis, G., Vournas, C.D.: 'Full-converter wind generator modelling for transient stability studies', *IEEE Trondheim PowerTech*, 2011, **1**, pp. 1–7
44 Leon, A.E., Solsona, J.A., Busada, C., Chiacchiarini, H., Valla, M.I.: 'High-performance control of a three-phase voltage-source converter including feedforward compensation of the estimated load current', *Energy Convers. Manage.*, 2009, **50**, (8), pp. 2000–2008
45 Slootweg, J.G., de Haan, S.W.H., Polinder, H., Kling, W.L.: 'General model for representing variable speed wind turbines in power system dynamics simulations', *IEEE Trans. Power Syst.*, 2003, **18**, (1), pp. 144–151
46 Salman, S.K., Teo, A.L.J.: 'Windmill modeling consideration and factors influencing the stability of a grid-connected wind power-based embedded generator', *IEEE Trans. Power Syst.*, 2003, **18**, (2), pp. 793–802
47 Blasco, V., Kaura, V.: 'A new mathematical model and control of a three-phase AC–DC voltage source converter', *IEEE Trans. Power Electron.*, 1997, **12**, (1), pp. 116–123
48 Kaura, V., Blasko, V.: 'Operation of a phase locked loop system under distorted utility conditions', *IEEE Trans. Ind. Appl.*, 1997, **33**, (1), pp. 58–63
49 Chung, S.-K.: 'A phase tracking system for three phase utility interface inverters', *IEEE Trans. Power Electron.*, 2000, **15**, (3), pp. 431–438
50 Sanchez-Gasca, J.J., Chow, J.H.: 'Power system reduction to simplify the design of damping controllers for interarea oscillations', *IEEE Trans. Power Syst.*, 1996, **11**, (3), pp. 1342–1349
51 Leon, A.E., Mauricio, J.M., Gomez-Exposito, A., Solsona, J.A.: 'Hierarchical wide-area control of power systems including wind farms and FACTS for short-term frequency regulation', *IEEE Trans. Power Syst.*, 2012, **27**, (4), pp. 2084–2092
52 Seo, J.-C., Kim, T.-H., Park, J.-K., Moon, S.-I.: 'An LQG based PSS design for controlling the SSR in power systems with series-compensated lines', *IEEE Trans. Energy Convers.*, 1996, **11**, (2), pp. 423–428
53 Ogata, K.: 'Modern control engineering' (Prentice-Hall, 1997)
54 Kamwa, I., Grondin, R., Hebert, Y.: 'Wide-area measurement based stabilizing control of large power systems-a decentralized/hierarchical approach', *IEEE Trans. Power Syst.*, 2001, **16**, (1), pp. 136–153
55 Pena, R., Clare, J.C., Asher, G.M.: 'Doubly fed induction generator using back-to-back PWM converters and its application to variable-speed wind-energy generation', *IEE Proc. Electr. Power Appl.*, 1996, **143**, (3), pp. 231–241
56 Wasynczuk, O.: 'Damping subsynchronous resonance using reactive power control', *IEEE Trans. Power Appar. Syst.*, 1981, **100**, (3), pp. 1096–1104
57 Leon, A.E., Solsona, J.A., Valla, M.I.: 'Control strategy for hardware simplification of VSC-based power applications', *IET Power Electron.*, 2011, **4**, (1), pp. 39–50
58 Taylor, C.W., Erickson, D.C., Martin, K.E., Wilson, R.E., Venkatasubramanian, V.: 'WACS–wide-area stability and voltage control system: R&D and online demonstration', *Proc. IEEE*, 2005, **93**, (5), pp. 892–906
59 Chow, J.J., Sanchez-Gasca, J.H., Ren, H., Wang, S.: 'Power system damping controller design-using multiple input signals', *IEEE Control Syst. Mag.*, 2000, **20**, (4), pp. 82–90
60 Joshi, S.R., Kulkarni, A.M.: 'Analysis of SSR performance of TCSC control schemes using a modular high bandwidth discrete-time dynamic model', *IEEE Trans. Power Syst.*, 2009, **24**, (2), pp. 840–848
61 Dotta, D., e Silva, A.S., Decker, I.C.: 'Wide-area measurements-based two-level control design considering signal transmission delay', *IEEE Trans. Power Syst.*, 2009, **24**, (1), pp. 208–216
62 Zabaiou, T., Dessaint, L.-A., Okou, F.-A., Grondin, R.: 'Wide-area coordinating control of SVCs and synchronous generators with signal transmission delay compensation'. IEEE Power and Energy Society General Meeting, 2010, pp. 1–9
63 Chaudhuri, B., Majumder, R., Pal, B.C.: 'Wide-area measurement-based stabilizing control of power system considering signal transmission delay', *IEEE Trans. Power Syst.*, 2004, **19**, (4), pp. 1971–1979
64 Zabaiou, T., Okou, F., Dessaint, L.-A., Akhrif, O.: 'Time-delay compensation of a wide-area measurements-based hierarchical voltage and speed regulator', *Can. J. Electr. Comput. Eng.*, 2008, **33**, (2), pp. 77–85
65 Chaudhuri, N.R., Ray, S., Majumder, R., Chaudhuri, B.: 'A new approach to continuous latency compensation with adaptive phasor power oscillation damping controller (POD)', *IEEE Trans. Power Syst.*, 2010, **25**, (2), pp. 939–946
66 Harb, A.M., Widyan, M.S.: 'Modern nonlinear theory as applied to SSR of the IEEE second benchmark model'. IEEE Power Tech Conf. Proc., June 2003, vol. 3, pp. 1–7

67 Wachtel, S., Hartge, S.: 'Technical and economical benefits of wind energy converters with FACTS capabilities for power system and the grid integration of wind power'. EWEC Conf., May 2007, pp. 1–8
68 Safonov, M.G., Chiang, R.Y.: 'A Schur method for balanced-truncation model reduction', *IEEE Trans. Autom. Control*, 1989, **34**, (7), pp. 729–733
69 Leon, A.E., Solsona, J.A.: 'Design of reduced-order nonlinear observers for energy conversion applications', *IET Control Theory Appl.*, 2010, **4**, (5), pp. 724–734

9 Appendix

9.1 Appendix 1

A linearised power system model can be written as

$$\dot{\boldsymbol{x}}^{n\times 1} = \boldsymbol{A}^{n\times n}\boldsymbol{x}^{n\times 1} + \boldsymbol{B}^{n\times p}\boldsymbol{u}^{p\times 1} \tag{19}$$

$$\boldsymbol{y}^{m\times 1} = \boldsymbol{C}^{m\times n}\boldsymbol{x}^{n\times 1} \tag{20}$$

where vector $\boldsymbol{x}$ stands for the state variables of the system; vector $\boldsymbol{y}$ represents measurements or states to be fed back; and $\boldsymbol{u} = [\Delta p_w\ \Delta q_w]^{\mathrm{T}}$ is the vector which contains the control inputs from the SSR damping controller. Matrix and vector dimensions are indicated as superscripts to clarify the transformations below, where n, p and m are the number of states, control inputs, and measurements, respectively.

Considering the system (19) and (20), and using the balanced model truncation through square root method, the following reduced model is obtained

$$\dot{\boldsymbol{w}}^{r\times 1} = \boldsymbol{S}_{\mathrm{L}}^{\mathrm{T}r\times n}\boldsymbol{A}^{n\times n}\boldsymbol{S}_{\mathrm{R}}^{n\times r}\boldsymbol{w}^{r\times 1} + \boldsymbol{S}_{\mathrm{L}}^{\mathrm{T}r\times n}\boldsymbol{B}^{n\times p}\boldsymbol{u}^{p\times 1} \tag{21}$$

$$\boldsymbol{y}^{m\times 1} = \boldsymbol{C}^{m\times n}\boldsymbol{S}_{\mathrm{R}}^{n\times r}\boldsymbol{w}^{r\times 1} \tag{22}$$

The derivation of (21) and (22) is addressed in Appendix 2. Further details of the reduction methodology can also be found in several works, for example [50, 68]. States $\boldsymbol{w}$ represent the internal states of the reduced model, where $r<n$ is the number of reduced states, and $\boldsymbol{S}_{\mathrm{L}}$ and $\boldsymbol{S}_{\mathrm{R}}$ are matrices which allow to reduce the power system model. When reduction methods are applied, although the reduced system behaves like the original system, from an input–output point of view ($\boldsymbol{u}\mapsto\boldsymbol{y}$), the reduced internal states $\boldsymbol{w}$ do not have physical meaning, and cannot be measured. In order to overcome this drawback, the transformation $\boldsymbol{T}^{m\times r} \triangleq \boldsymbol{C}^{m\times n}\boldsymbol{S}_{\mathrm{R}}^{n\times r}$ is proposed. Note that, if a number of measured states equal to the number of reduced internal states is chosen ($m=r$), then $\boldsymbol{T}^{m\times r}$ will be a square matrix, and from (22) the transformation $\boldsymbol{w}\mapsto\boldsymbol{y}$ will be reliable. This transformation allows to write the reduced model with $\boldsymbol{y}$ as dynamic states. Therefore applying the transformation $\boldsymbol{T}^{m\times r}$ to the system (21) results

$$\dot{\boldsymbol{y}} = \boldsymbol{T}\boldsymbol{S}_{\mathrm{L}}^{\mathrm{T}}\boldsymbol{A}\boldsymbol{S}_{\mathrm{R}}\boldsymbol{T}^{-1}\boldsymbol{y} + \boldsymbol{T}\boldsymbol{S}_{\mathrm{L}}^{\mathrm{T}}\boldsymbol{B}\boldsymbol{u} \tag{23}$$

The origin of the transformation $\boldsymbol{T}^{m\times r}$ and details of the calculation of (23) are given in the second subsection of Appendix 2.

9.2 Appendix 2: Square root balance truncation algorithm

In this Appendix, the balanced model truncation via square root method to calculate an r-order reduced model from an n-order model, where $r<n$ is presented. This algorithm is a four-stage procedure. The original n-order system is given by

$$\dot{\boldsymbol{x}} = \boldsymbol{A}\boldsymbol{x} + \boldsymbol{B}\boldsymbol{u} \tag{24}$$

$$\boldsymbol{y} = \boldsymbol{C}\boldsymbol{x} + \boldsymbol{D}\boldsymbol{u} \tag{25}$$

First, we obtain the controllability ($\boldsymbol{W}_{\mathrm{c}}$) and observability ($\boldsymbol{W}_{\mathrm{o}}$) grammians defined by [53]

$$\boldsymbol{W}_{\mathrm{c}} = \int_0^{\infty} \mathrm{e}^{\boldsymbol{A}\tau}\boldsymbol{B}\boldsymbol{B}^{\mathrm{T}}\mathrm{e}^{\boldsymbol{A}^{\mathrm{T}}\tau}\,\mathrm{d}\tau \tag{26}$$

$$\boldsymbol{W}_{\mathrm{o}} = \int_0^{\infty} \mathrm{e}^{\boldsymbol{A}^{\mathrm{T}}\tau}\boldsymbol{C}^{\mathrm{T}}\boldsymbol{C}\mathrm{e}^{\boldsymbol{A}\tau}\,\mathrm{d}\tau \tag{27}$$

They can be calculated by solving the following continuous-time Lyapunov equations

$$\boldsymbol{A}\boldsymbol{W}_{\mathrm{c}} + \boldsymbol{W}_{\mathrm{c}}\boldsymbol{A}^{\mathrm{T}} + \boldsymbol{B}\boldsymbol{B}^{\mathrm{T}} = \boldsymbol{0} \tag{28}$$

$$\boldsymbol{A}^{\mathrm{T}}\boldsymbol{W}_{\mathrm{o}} + \boldsymbol{W}_{\mathrm{o}}\boldsymbol{A} + \boldsymbol{C}^{\mathrm{T}}\boldsymbol{C} = \boldsymbol{0} \tag{29}$$

It is easily achieved using the 'gram' or 'hksv' commands of MatLab.

Second, we find the singular-value decomposition (SVD) of the controllability and observability grammians ('svd' command), resulting

$$\mathbf{W}_{\mathrm{c}} = \mathbf{U}_{\mathrm{c}}\boldsymbol{\Sigma}_{\mathrm{c}}\mathbf{V}_{\mathrm{c}}^{\mathrm{T}} \tag{30}$$

$$\mathbf{W}_{\mathrm{o}} = \mathbf{U}_{\mathrm{o}}\boldsymbol{\Sigma}_{\mathrm{o}}\mathbf{V}_{\mathrm{o}}^{\mathrm{T}} \tag{31}$$

The following matrices are also computed

$$\boldsymbol{L}_{\mathrm{c}} = \boldsymbol{U}_{\mathrm{c}}\boldsymbol{\Sigma}_{\mathrm{c}}^{1/2} \tag{32}$$

$$\boldsymbol{L}_{\mathrm{o}} = \boldsymbol{U}_{\mathrm{o}}\boldsymbol{\Sigma}_{\mathrm{o}}^{1/2} \tag{33}$$

Third, we obtain the SVD of the matrix $\boldsymbol{L}_{\mathrm{o}}^{\mathrm{T}}\boldsymbol{L}_{\mathrm{c}}$, yielding

$$\boldsymbol{L}_{\mathrm{o}}^{\mathrm{T}}\boldsymbol{L}_{\mathrm{c}} = \boldsymbol{U}\boldsymbol{\Sigma}\boldsymbol{V}^{\mathrm{T}} \tag{34}$$

Fourth, the left and right transformations for the r-order reduced model are determined by ('balsq' command)

$$\mathbf{S}_{\mathrm{R}} = \mathbf{L}_{\mathrm{c}}\mathbf{V}_{(:,1:r)}\boldsymbol{\Sigma}_{(1:r,1:r)}^{-1/2} \tag{35}$$

$$\mathbf{S}_{L} = \mathbf{L}_{o}\mathbf{U}_{(:,1:r)}\boldsymbol{\Sigma}_{(1:r,1:r)}^{-1/2} \tag{36}$$

where the nomenclature (:,1: r) states that the matrix $\boldsymbol{V}_{(:,1:r)}$ consist of all rows and the first r columns from the matrix $\boldsymbol{V}$.

Finally, the r-order reduced model is given by

$$\dot{\boldsymbol{w}} = \boldsymbol{S}_{\mathrm{L}}^{\mathrm{T}}\boldsymbol{A}\boldsymbol{S}_{\mathrm{R}}\boldsymbol{w} + \boldsymbol{S}_{\mathrm{L}}^{\mathrm{T}}\boldsymbol{B}\boldsymbol{u} \tag{37}$$

$$\boldsymbol{y} = \boldsymbol{C}\boldsymbol{S}_{\mathrm{R}}\boldsymbol{w} + \boldsymbol{D}\boldsymbol{u} \tag{38}$$

which can also be obtained with the 'balancmr' command of MatLab. States $\boldsymbol{w}$ represent the internal states of the reduced model. The proof of the square root balance truncation algorithm can be found in [68].

9.2.1 Transformation of the reduced state: In the following lines, it is shown how the reduced model (37) can be transformed to have the variables $\boldsymbol{y}$ (with physical meaning) as dynamic states instead of the variables $\boldsymbol{w}$ (with

doi: 10.1049/iet-gtd.2012.0357

nonphysical meaning). If we consider $\boldsymbol{D} = \boldsymbol{0}$ (which is valid in the studied power system) then, from (38), a transformation from $\boldsymbol{w}$ to $\boldsymbol{y}$ can be obtained

$$\boldsymbol{y} = \boldsymbol{C}\boldsymbol{S}_{\mathrm{R}}\boldsymbol{w} \tag{39}$$

This transformation $\boldsymbol{y} = \boldsymbol{T}\boldsymbol{w}$ is defined from (39) as

$$\boldsymbol{T} \triangleq \boldsymbol{C}\boldsymbol{S}_{\mathrm{R}} \tag{40}$$

If the transformation $\boldsymbol{T}$ is invertible, then we can write its inverse transformation

$$\boldsymbol{w} = \boldsymbol{T}^{-1}\boldsymbol{y} \tag{41}$$

and taking the time derivative results

$$\dot{\boldsymbol{w}} = \boldsymbol{T}^{-1}\dot{\boldsymbol{y}} \tag{42}$$

Using (41) and (42) in (37), we obtain

$$\boldsymbol{T}^{-1}\dot{\boldsymbol{y}} = \boldsymbol{S}_{\mathrm{L}}^{\mathrm{T}}\boldsymbol{A}\boldsymbol{S}_{\mathrm{R}}\boldsymbol{T}^{-1}\boldsymbol{y} + \boldsymbol{S}_{\mathrm{L}}^{\mathrm{T}}\boldsymbol{B}\boldsymbol{u} \tag{43}$$

Finally, premultiplying by $\boldsymbol{T}$ both sides of (43), we arrive to the reduced model with dynamic states $\boldsymbol{y}$, which was used in (16) and (23)

$$\underbrace{\boldsymbol{T}\boldsymbol{T}^{-1}}_{\mathbf{I}}\dot{\boldsymbol{y}} = \boldsymbol{T}\boldsymbol{S}_{\mathrm{L}}^{\mathrm{T}}\boldsymbol{A}\boldsymbol{S}_{R}\boldsymbol{T}^{-1}\boldsymbol{y} + \boldsymbol{T}\boldsymbol{S}_{\mathrm{L}}^{\mathrm{T}}\boldsymbol{B}\boldsymbol{u} \tag{44}$$

9.3 Appendix 3

From the dynamics of the multi-mass system (6) and taking into account (5), the multi-mass system can be rewritten as

$$\dot{\boldsymbol{x}} = \boldsymbol{A}_{\mathrm{m}}\boldsymbol{x} + \boldsymbol{B}_{\mathrm{te}}T_{\mathrm{e}} + \boldsymbol{B}_{\mathrm{tm}}T_{\mathrm{m}} \tag{45}$$

where the following vectors are defined

$$\boldsymbol{B}_{\mathrm{te}} \triangleq \boldsymbol{B}_{\mathrm{m}}\begin{bmatrix} 0 & -1 & 0 & 0 \end{bmatrix}^{\mathrm{T}} \tag{46}$$

$$\boldsymbol{B}_{\mathrm{tm}} \triangleq \boldsymbol{B}_{\mathrm{m}}\begin{bmatrix} 0 & 0 & \frac{1}{2} & \frac{1}{2} \end{bmatrix}^{\mathrm{T}} \tag{47}$$

Since in large synchronous generators the stator resistance loss is small, the electromagnetic torque T_{e} can be approximated by the electric power measurement in the per-unit system $T_{\mathrm{e}} \cong P_{\mathrm{e}}$ $(\omega \cong 1)$. However, the mechanical torque T_{m} is not usually sensed; consequently, it will also be estimated. In order to include T_{m} as an observer state, a smoothly varying mechanical torque model is assumed $(\dot{T}_{\mathrm{m}} \cong 0)$. Therefore the system (45) can be extended to

$$\dot{\boldsymbol{x}}_{\mathrm{e}} = \boldsymbol{A}_{\mathrm{e}}\boldsymbol{x}_{\mathrm{e}} + \boldsymbol{B}_{\mathrm{e}}T_{\mathrm{e}} \tag{48}$$

$$\boldsymbol{y} = \boldsymbol{C}_{\mathrm{e}}\boldsymbol{x}_{\mathrm{e}} = \begin{bmatrix} \omega_1 & \omega_4 \end{bmatrix}^{\mathrm{T}} \tag{49}$$

where a new extended state vector $\boldsymbol{x}_{\mathrm{e}} = [\boldsymbol{x}\, T_{\mathrm{m}}]^{\mathrm{T}}$ is defined along with the following extended matrices

$$\boldsymbol{A}_{\mathrm{e}} \triangleq \begin{bmatrix} \boldsymbol{A}_{\mathrm{m}} & \boldsymbol{B}_{\mathrm{tm}} \\ \boldsymbol{0} & \boldsymbol{0} \end{bmatrix}, \quad \boldsymbol{B}_{\mathrm{e}} \triangleq \begin{bmatrix} \boldsymbol{B}_{\mathrm{te}} \\ 0 \end{bmatrix} \tag{50}$$

$$\boldsymbol{C}_{\mathrm{e}} \triangleq \begin{bmatrix} \boldsymbol{C}_{\mathrm{m}} & \boldsymbol{0} \end{bmatrix} \tag{51}$$

$$\boldsymbol{C}_{\mathrm{m}} \triangleq \begin{bmatrix} 0 & 0 & 0 & 1 & 0 & 0 & 0 \\ 0 & 0 & 0 & 0 & 0 & 0 & 1 \end{bmatrix} \tag{52}$$

Based on the model (48) and (49) a Luenberger observer is proposed [53, 69]. Therefore the observer dynamics is built as follows

$$\dot{\hat{\boldsymbol{x}}}_{\mathrm{e}} = \boldsymbol{A}_{\mathrm{e}}\hat{\boldsymbol{x}}_{\mathrm{e}} + \boldsymbol{B}_{\mathrm{e}}T_{\mathrm{e}} + \boldsymbol{G}_{\mathrm{e}}\left(\boldsymbol{y} - \boldsymbol{C}_{\mathrm{e}}\hat{\boldsymbol{x}}_{\mathrm{e}}\right) \tag{53}$$

where the symbol (^)is used to indicate an estimated value, and the gain matrix $\boldsymbol{G}_{\mathrm{e}} \in \mathbb{R}^{2n\times 2}$ should be chosen to guarantee that the estimation error converges to zero. To find the matrix $\boldsymbol{G}_{\mathrm{e}}$ firstly, we define the estimation error $\boldsymbol{e} \triangleq \boldsymbol{x}_{\mathrm{e}} - \hat{\boldsymbol{x}}_{\mathrm{e}}$, then the estimation error dynamics is obtained by subtracting (53) from (48); consequently, $\dot{\boldsymbol{e}} = \left(\boldsymbol{A}_{\mathrm{e}} - \boldsymbol{G}_{\mathrm{e}}\boldsymbol{C}_{\mathrm{e}}\right)\boldsymbol{e}$. Finally, the matrix $\boldsymbol{G}_{\mathrm{e}}$ can be designed using linear techniques such as eigenvalue placement or optimal quadratic regulation; the latter is used in our design [53]. In this way, when the matrix $\boldsymbol{A}_{\mathrm{e}} - \boldsymbol{G}_{\mathrm{e}}\boldsymbol{C}_{\mathrm{e}}$ has stable eigenvalues the estimation error converges to zero in an exponential manner.

The weight matrices in the optimal quadratic regulation design were chosen as $\boldsymbol{Q} = 10^3\ \mathrm{diag}([\boldsymbol{I}^{7\times 7},\ 4000])$ and $\boldsymbol{R} = \boldsymbol{I}^{2\times 2}$; then, solving the optimal quadratic problem (using the 'lqr' command of MatLab), the observer gain matrix is obtained

$$\boldsymbol{G}_{\mathrm{e}} = \begin{bmatrix} -71.0 & 71.1 & -29.4 & 294 & 112 & 2.30 & 19.6 & 3565 \\ -71.1 & -29 & 138 & 19.6 & 45.6 & 41.8 & 187 & 5223 \end{bmatrix}^{\mathrm{T}} \tag{54}$$